



## OPEN

## Generation of proton aurora by magnetosonic waves

## SUBJECT AREAS:

MAGNETOSPHERIC  
PHYSICS

ASTROPHYSICAL PLASMAS

MAGNETICALLY CONFINED  
PLASMAS

AURORA

Fuliang Xiao<sup>1</sup>, Qiugang Zong<sup>2</sup>, Yongfu Wang<sup>2</sup>, Zhaoguo He<sup>3</sup>, Zhenpeng Su<sup>4</sup>, Chang Yang<sup>1</sup>  
& Qinghua Zhou<sup>1</sup>

<sup>1</sup>School of Physics and Electronic Sciences, Changsha University of Science and Technology, Changsha 410004, China, <sup>2</sup>School of Earth and Space Sciences, Peking University, Beijing 100871, China, <sup>3</sup>Center for Space Science and Applied Research, Chinese Academy of Sciences, Beijing, 100190, China, <sup>4</sup>Chinese Academy of Sciences Key Laboratory for Basic Plasma Physics, University of Science and Technology of China, Hefei 230026, China.

Received

19 December 2013

Accepted

16 May 2014

Published

5 June 2014

Correspondence and requests for materials should be addressed to F.L.X. (flxiao@126.com) or Q.G.Z. (qgzong@pku.edu.cn)

Earth's proton aurora occurs over a broad MLT region and is produced by the precipitation of low-energy (2–10 keV) plasmasheet protons. Proton precipitation can alter chemical compositions of the atmosphere, linking solar activity with global climate variability. Previous studies proposed that electromagnetic ion cyclotron waves can resonate with protons, producing proton scattering precipitation. A long-outstanding question still remains whether there is another mechanism responsible for the proton aurora. Here, by performing satellite data analysis and diffusion equation calculations, we show that fast magnetosonic waves can produce trapped proton scattering that yields proton aurora. This provides a new insight into the mechanism of proton aurora. Furthermore, a ray-tracing study demonstrates that magnetosonic wave propagates over a broad MLT region, consistent with the global distribution of proton aurora.

Earth's proton aurora is formed when charged protons precipitate into the atmosphere loss cone, within a few degrees at the equator, and subsequently collide with the neutral atmosphere at low altitudes<sup>1</sup>. Proton aurora can provide important information for understanding magnetosphere-ionosphere interaction by supplementing the direct imaging of the magnetosphere<sup>2</sup>. Since charged protons are easily trapped inside the Earth's magnetic field due to a minimum magnetic field existing at the equator, such proton precipitation requires a scattering mechanism to break the first adiabatic invariant. In the basically collisionless and tenuous magnetosphere, interactions between protons and plasma waves can induce such non-adiabatic scattering. One important plasma wave, electromagnetic ion cyclotron (EMIC) wave can interact with protons and efficiently scatter protons into the atmosphere<sup>3–6</sup>. However, strong EMIC waves are present primarily along the plasma plume in the duskside<sup>7–9</sup> and on the dayside in the outer magnetosphere  $L > 6^{10–12}$ . This appears to be difficult for EMIC wave alone to explain the broad MLT distribution of proton auroral emission from the morning sector to the dusk sector associated with the precipitating protons at lower  $L$ -shells. Hence, the fundamental and long-outstanding problem as to what mechanism is primarily responsible for proton auroral emission still remains unresolved. Another important wave, fast magnetosonic (MS) wave, also named equatorial noise<sup>13</sup>, can resonate with protons, potentially leading to rapid pitch angle scattering of protons. Furthermore, MS waves can propagate eastward (later MLT) or westward (earlier MLT) over a broad region of MLT<sup>14–16</sup>. However, it has not been possible so far to determine whether MS wave is indeed another generating mechanism of the proton aurora, because simultaneous observations concerning MS wave activity, proton pitch distribution and proton auroral emissions are challenging due to extremely difficult observational conditions. Fortunately, such simultaneous observations were serendipitously found in the unique events on September 16, 2003, to identify such mechanism.

## Results

On September 16, 2003 an interplanetary coronal mass ejection (CME) interacted with the Earth's magnetosphere, leading to a small geomagnetic storm ( $D_{st} \approx -50$  nT). The Cluster spacecrafts, which stayed around the noon near the Earth's equator for about ten minutes then, recorded strong MS wave activities for a duration of  $\sim 10$  minutes in the frequency range  $\sim 10$ –150 Hz and around the noon local time sector from 11.47 to 11.41 MLT (Fig. 1a). MS wave is confined within a few degrees of the geomagnetic equator and exhibits a notable harmonic structure, viz., spaced at  $4f_{cp}$  and  $12f_{cp}$  (Fig. 1a). Moreover, MS wave has a normal angle  $\theta \approx 90^\circ$  (Fig. 1b) and an ellipticity  $\approx 0$  (Fig. 1c), implying that MS wave propagates very obliquely with respect to the ambient magnetic field direction<sup>17</sup>.

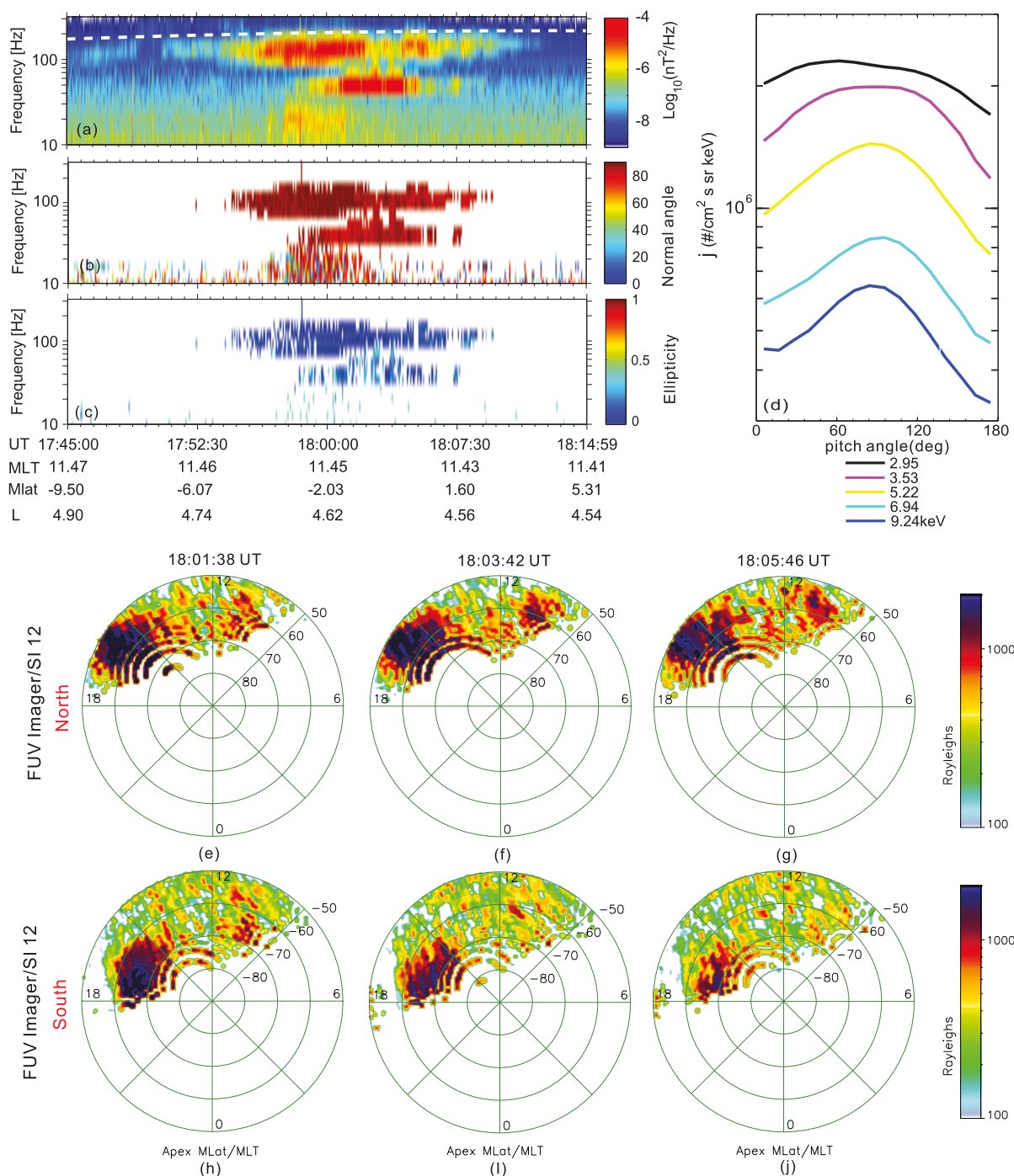


**Figure 1 | Satellite data on 16 September 2003 storm.** Data collected by the Cluster STAFF instrument during  $\sim 10$  minutes duration for MS wave power (a), wave normal angle (b), the angle between the Earth's magnetic field and the normal to the plane of the wave; and wave ellipticity (c), the degree of elliptical polarization. MS waves are right hand polarized electromagnetic waves which occur as a series of narrow tones, spaced at multiples of the proton gyrofrequency  $f_{cp}$  up to the lower hybrid resonance frequency  $f_{LH}$ . a, MS waves maximizes basically at frequencies from  $\sim 10$ –150 Hz, spaced at  $4f_{cp}$  ( $f_{cp} \approx 5$  Hz) and  $12f_{cp}$ . The white dotted line denotes the lower hybrid resonance frequency  $f_{LH}$ . b–c, The observed waves have a high normal angle  $\theta \approx 90^\circ$  and a high degree of elliptical polarization (ellipticity  $\approx 0$ ), indicating that the k vector is approximately perpendicular to the ambient magnetic field direction. d, Pitch angle distribution of protons for different indicated energies (2–10 keV) measured by CIS instrument. Proton fluxes peak at a pitch angle of  $90^\circ$  and drop dramatically at small pitch angles. e–j, Auroral snapshots for northern hemisphere and southern hemisphere as a function of magnetic local time (MLT) and magnetic latitude (MLat) obtained by FUV-SI12 onboard IMAGE spacecraft when IMAGE spacecraft travels at the location  $\sim 15$  Mlat and altitude  $= 8 R_E$ . Proton aurora bands are present from the morning sector to dusk sector 09:00–18:00 MLT, with the strongest emission basically in 14:00–18:00 MLT. The auroral emission is asymmetric with a more intensity and a broader latitude in the northern hemisphere than those in the southern hemisphere.

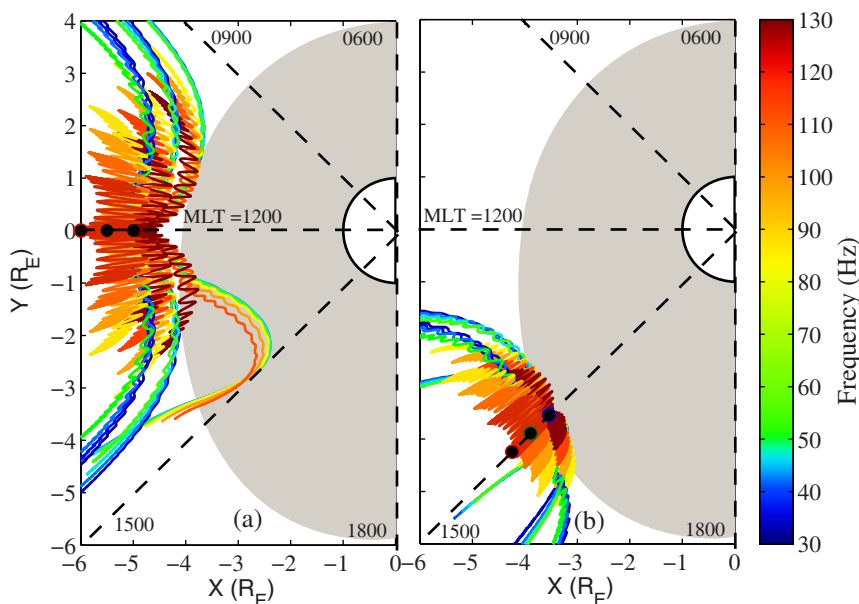


**Figure 2 | Ray-tracing of MS waves.** Ray paths representing MS waves are initiated at the equator, at MLT=12:00 (a) and 15:00 (b), with the ray-tracing parameters as shown in Table 1. The corresponding color scale indicates the initial wave frequency of each ray in Hz. The black circles indicate the initial positions  $L = 5.0, 5.5$  and  $6.0$ , where  $L$  is the distance in Earth radii ( $1R_E = 6,370$  km) from the centre of the Earth to the equatorial crossing of a given magnetic field line. MS waves can propagate eastward (later MLT) or westward (earlier MLT) basically from the morning sector to the dusk sector 0900–1800 MLT, corresponding to the occurrence of proton auroral emission.

Figure 1d shows a pancake distribution of proton flux for different indicated energies (2–10 keV) measured by CIS instrument. Proton flux maximizes at a pitch angle of  $90^\circ$  and drops remarkably at small pitch angles at each energy, particularly for energy above 3.53 keV. Since a pancake distribution is produced when protons with smaller pitch angles have been scattered into the loss cone, any endeavor to identify whether MS waves are really responsible for proton auroral precipitation must also explain the formation of pancake distributions.

Figure 1e–j show auroral snapshots observed by FUV-SI12 instrument onboard IMAGE spacecraft<sup>18</sup> for the northern hemisphere and southern hemisphere produced by the precipitation of 2–10 keV protons originating from the plasma sheet. The SI12 instrument detects the Doppler-shifted Lyman- $\alpha$  photons corresponding to precipitating charge-exchanged protons with energies of a few keV<sup>19,20</sup>. Proton aurora covers a broad MLT region 09:00–18:00 MLT, with stronger emissions roughly in 14:00–18:00 MLT. Such a broad MLT distribution of proton aurora requires MS waves which can produce proton scattering to occur over a similar broad MLT region.

Unfortunately, there is no direct wave data over such a broad MLT region during this event. Here, we adopt the previously developed programs<sup>21,22</sup> to trace MS waves with different frequencies based on the wave data (Fig. 1a–b). MS waves are launched at 12:00 and 15:00 MLT for different locations at the geomagnetic equator. The modeled results (Fig. 2) confirm that MS waves can indeed propagate over the similar MLT region from the morning sector to the dusk sector 09:00–18:00 MLT.

Resonant interactions between MS waves and protons take place when the wave frequency equals a multiple of the proton gyrofrequency in the proton reference frame. These cyclotron MS-proton interactions produce efficient exchange of energy and momentum between waves and protons, leading to stochastic proton scattering. Such stochastic scattering can be evaluated in terms of pitch angle and momentum diffusion coefficients induced by cyclotron MS-proton interactions. Then, the dynamic evolution of the proton distribution function can be calculated by solving the Fokker-Planck diffusion equation associated with pitch-angle and momentum

diffusion coefficients<sup>23</sup>. Here, we use this method to model evolutions of the proton distribution following their injection into the magnetosphere.

Calculation of the diffusion coefficients requires a detailed knowledge of the amplitudes and spectral properties of the waves. A standard way is to assume that the wave spectral density obey a Gaussian distribution in wave frequency and wave normal angle<sup>24</sup> (see the details in Methods). To allow the data fitting more reasonable, we

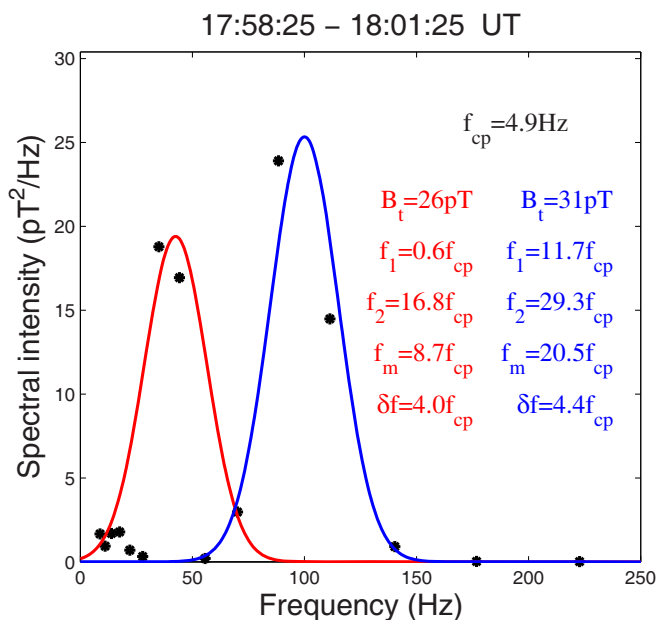


**Figure 3 | Gaussian Fitting curves.** The modeled Gaussian fit (solid) to the observed two-band wave spectra (dot) over a three-minute period 17:58:25–18:01:25 is shown, together with the fitted wave amplitudes  $B_t$ , the peak wave frequencies  $f_m$ , the bandwidths  $\delta f$ , the lower and upper bands  $f_1$  and  $f_2$ .

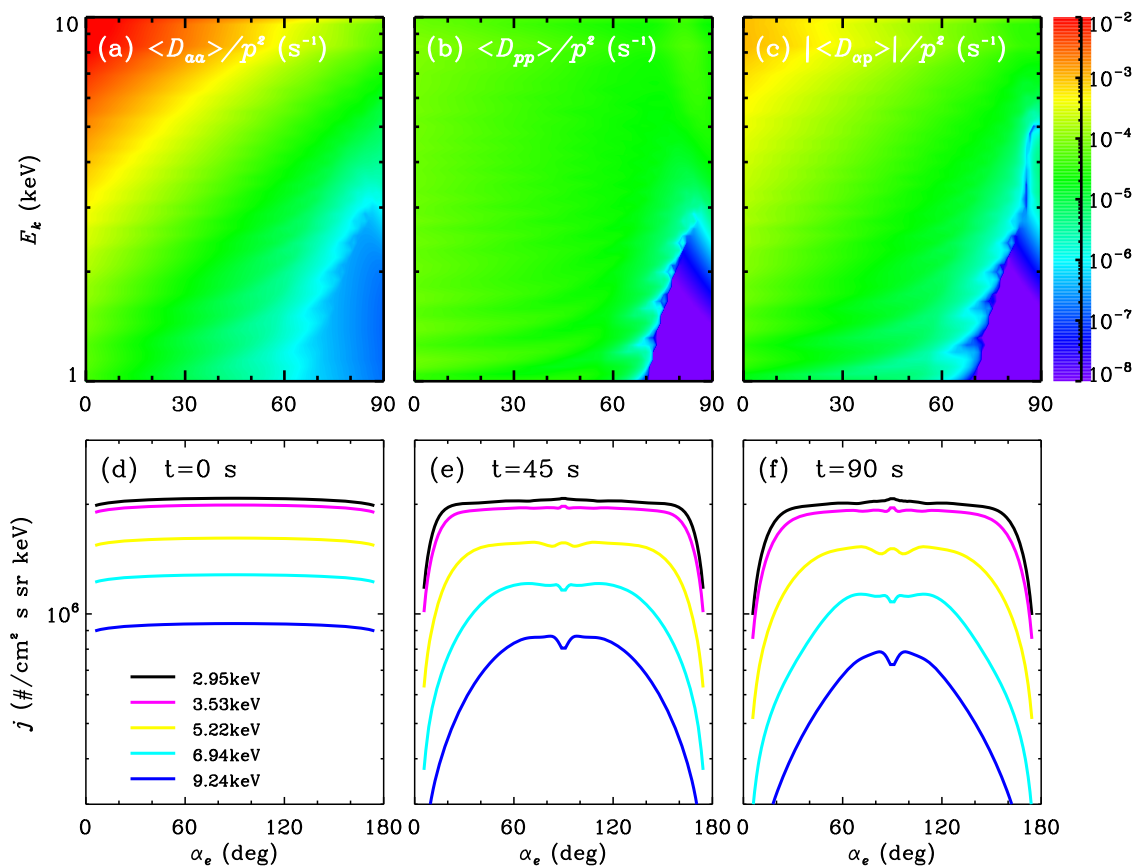


**Figure 4 | Diffusion rates Proton bounce-averaged pitch angle ( $\langle D_{aa} \rangle$ , a), momentum ( $\langle D_{pp} \rangle$ , b) and cross ( $\langle D_{ap} \rangle$ , c) diffusion rates for resonant MS wave interactions with protons. Pitch angle  $\langle D_{aa} \rangle$  and cross  $\langle D_{ap} \rangle$  are respectively higher than momentum  $\langle D_{pp} \rangle$ . Combined scattering by all three diffusion rates leads to rapid pitch-angle scattering between 2 and 10 keV at lower pitch angles and the resultant proton auroral precipitation into the atmosphere on a timescale comparable to tens of seconds. **Evolution of the proton flux** Starting with an initial condition representative of protons (d), we show the proton flux due to scattering by MS waves from a numerical solution to the two-dimensional Fokker-Planck diffusion equation. MS wave causes a rapid loss of low-energy (2–10 keV) protons within tens of seconds (e–f), leading to the strongest proton auroral precipitation from the morning sector to the dusk sector 0900–1800 MLT.**

average the observed wave magnetic field intensity over the indicated time period in this event and then present a least squares Gaussian fit to the observed two-band spectral intensity (Fig. 1a), together with the corresponding fitting parameters as shown in Figure 3. We then calculate bounce-averaged diffusion coefficients for MS waves as shown in Figure 4a–c. All the diffusion coefficients cover a broad region of pitch angle and energy, with high values at lower pitch angles. In particular, the pitch angle diffusion rate above  $\sim 7$  keV can approach 0.01/s around the loss-cone, allowing efficient pitch scattering of protons into the loss-cone in a time scale of tens of seconds. Moreover, pitch angle and cross diffusion coefficients are higher than momentum diffusion coefficients particularly at lower pitch angles, implying that pitch angle diffusion dominates over the energy diffusion while cross diffusion coefficients should also contribute to proton-MS interaction.

Using those diffusion rates in Figure 4a–c, we solve a two-dimensional Fokker-Planck diffusion equation by a recently introduced hybrid difference method<sup>25</sup> and calculate phase space density  $f$  evolution of protons due to MS waves. We then simulate the evolution of differential flux  $j$  by the subsequent conversion  $j = p^2 f$  and extend the results to the range of  $90^\circ$ – $180^\circ$  due to the mirror symmetry. The results (Fig. 4d–f) confirm that MS waves can produce a rapid pitch angle scattering of protons within tens of seconds and substantially modify the entire population of injected protons, leading to the formation of pancake distributions at energies 2–10 keV. It should be mentioned that anomalous depressions (or dips) occur around

$90^\circ$  because of the absence of resonant scattering at (or around)  $90^\circ$ . Moreover, the diffusion rates around  $90^\circ$  are very small in the energy range 1–3 keV and gradually increase above 3 keV. Consequently, those dips around the pitch angle  $90^\circ$  are more noticeable when energy increases (Fig. 4a–c). Although our simulation results are sensitively dependent on adopted model parameters and display anomalous depressions around  $90^\circ$ , the dominant features of Figure 4f are very similar to the Cluster data shown in Figure 1d. Considering that MS waves can propagate over a broad MLT region in this event (Fig. 2), we therefore conclude that MS waves are indeed responsible for the precipitation of energetic protons into the atmosphere, producing the resultant proton aurora (Fig. 1e–j).

## Discussion

The simultaneous observation and corresponding modeling presented in this study firstly link MS waves to the origin of proton aurora. Our results definitively demonstrate that, as presented in Fig. 5, MS waves can produce rapid proton precipitation responsible for proton aurora, naturally accounting for the remnant pancake proton distribution left behind in space and the broad MLT distribution of proton aurora. Although our simulations were performed around the noon 11:30 MLT, this conclusion should be valid over the entire region of excited MS waves since the basic properties of MS-proton interaction should not change no matter whether the amplitude and morphology of MS waves are different under different locations.



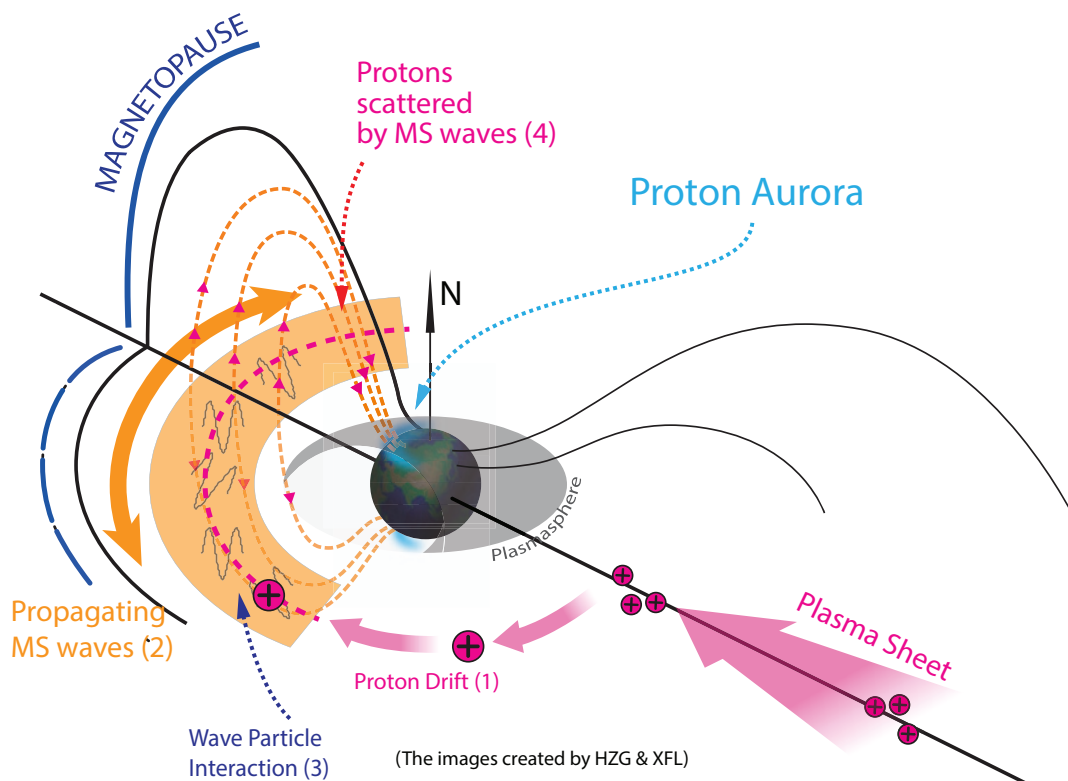


**Figure 5 | Protons scattered by MS waves.** Schematic diagram showing the solar wind protons, MS waves and the proton aurora. The image of the Earth was created by HZG and XFL. (1) The energetic protons originating from the plasmasheet are trapped in the Earth’s magnetic field and drift westward around the Earth. (2) MS waves propagate eastward or westward over a broad region from the morning side to the dusk side. (3) Wave-particle interaction occurs in the same region. (4) It acts as an unexpected mechanism to scatter the trapped protons into the atmosphere, yielding the proton aurora.

As shown in Figure 1, the proton auroral emission maximizes in the afternoon sector, which appears to be inconsistent with the recent statistical survey of MS waves observed on THEMIS spacecraft<sup>26</sup> that such waves are strongest in the dawn to pre-noon sector. However, the proton aurora emission intensity primarily depends on two factors: the number of the precipitating protons and the MS wave intensity. Since the precipitating protons originating from the plasma sheet drift westwards around the Earth (see Fig. 5), the protons encounter resonance with the afternoon sector MS waves at first, allowing part of protons precipitating into the atmosphere. Then the rest of protons continue resonating with MS waves on other sectors in their drifting. Moreover, the potentially existing plume EMIC waves along the duskside (though not observed directly here) may also contribute to the proton scattering. This probably explains why the proton aurora peak in the afternoon sector, instead of in the dawn to pre-noon sector.

It should be pointed out that, we use the quasi-linear theory of wave-particle interaction. Analogous to the Particle-in-cell treatment, the quasi-linear theory has been frequently adopted by the space plasma physics and magnetosphere research community to treat wave-particle interaction. The quasi-linear theory is valid by assuming that each individual particle randomly walks in velocity space, resonates with a succession of uncorrelated waves, and is scattered in a small amount in pitch angle and energy each time. Those conditions are basically satisfied in the Earth’s radiation belts for naturally generated MS waves, where the bandwidth is generally above the proton cyclotron frequency up to the lower hybrid frequency. Moreover, this study is intended to propose a new mechanism of proton aurora by MS-driven scattering, but not to exclude EMIC waves as a potential wave responsible for the proton scattering. The relative contribution

to the proton aurora emission from MS or EMIC waves deserves a future study.

Finally, in a departure from the previous works<sup>27</sup>, we focus on the pitch-angle scattering by the MS waves instead of the instability of MS waves in this study. The enhanced MS waves appear to be excited by those injected anisotropic protons with a typical ring distribution at energies of  $\sim 10$  keV or above prior to this event. Unfortunately, there is no direct data on MS waves or energetic proton distributions before this event because the Cluster satellite doesn’t stay in the radiation belt. We leave the instability of MS waves to a future study.

## Methods

The ray tracing of waves is performed by using the following standard Hamiltonian equations<sup>28</sup>:

$$\frac{d\mathbf{R}}{dt} = -\frac{\partial D}{\partial \mathbf{k}} / \frac{\partial D}{\partial \omega} \quad (1)$$

$$\frac{d\mathbf{k}}{dt} = \frac{\partial D}{\partial \mathbf{R}} / \frac{\partial D}{\partial \omega}, \quad (2)$$

where  $\mathbf{R}$ ,  $\omega$ ,  $\mathbf{k}$ , and  $t$  represent the position vector of a point on the ray path, the wave frequency, the wave vector, and the group time, respectively. The wave dispersion relation  $D(\mathbf{R}, \omega, \mathbf{k}) = 0$  at every point along the ray path, has well been documented in the previous work. The spatial variation in  $D$  can be written:

$$\frac{\partial D}{\partial \mathbf{R}} = \frac{\partial D}{\partial \mathbf{B}_0} \frac{\partial \mathbf{B}_0}{\partial \mathbf{R}} + \frac{\partial D}{\partial N_c} \frac{\partial N_c}{\partial \mathbf{R}} + \frac{\partial D}{\partial \mathbf{k}} \frac{\partial \mathbf{k}}{\partial \mathbf{R}} \quad (3)$$

where  $\mathbf{B}_0$  is an ambient magnetic field and  $N_c$  is the background plasma density.

Here, two Cartesian coordinate systems are adopted for the ray-tracing calculation<sup>15,21</sup>. The first is Earth centered Cartesian coordinate system (OXYZ), in which Z axis points north along the geomagnetic axis; and the X and Y axes stay in the geomagnetic axis equatorial plane. The second is a local Cartesian system, in which



Table 1 | Parameters for Ray Tracing

L	f/f <sub>cp</sub>	f(Hz)
5.0	11, 12, 13, 14, 23, 27, 31, 35	41.8, 45.5, 49.3, 53.0, 87.2, 102.4, 117.5, 132.7
5.5	12, 14, 16, 18, 30, 35, 40, 45	34.2, 39.8, 45.5, 51.2, 85.4, 99.7, 113.9, 128.2
6.0	16, 18, 20, 22, 40, 45, 50, 55	35.1, 39.5, 43.9, 48.0, 87.8, 98.7, 109.7, 120.7

the z axis points along the direction of the ambient magnetic field, the x axis is orthogonal to the z axis and stays in the meridian plane pointing away from the Earth at the equator, and the y axis completes the right-handed set. The wave vector  $\mathbf{k}$  makes an angle  $\theta$  with the z axis and the projection of  $\mathbf{k}$  onto the xy plane makes an angle  $\eta$  with the x axis, viz.,  $\mathbf{k} = k \cos \theta \mathbf{z} + k \sin \theta \cos \eta \mathbf{x} + k \sin \theta \sin \eta \mathbf{y}$ .  $\eta = 0^\circ, 90^\circ, 180^\circ$  and  $270^\circ$  correspond to the perpendicular component  $\mathbf{k}_\perp$  pointing away from the Earth, toward later MLT (eastward), toward the Earth, and toward earlier MLT (westward), respectively.

For ray-tracing, we adopt a dipole magnetic field model and the global core plasma density model<sup>29</sup>. Considering that MS wave propagate very obliquely, we choose the initial wave normal angle  $\theta = 88^\circ$ , and the initial azimuthal angle  $\eta = 150^\circ$  (toward earlier MLT) and  $30^\circ$  (toward later MLT). The other ray-tracing parameters for different wave frequencies and source locations are shown in Table 1.

To calculate the diffusion rates, we assume that the MS wave spectral density  $B_f^2$  follows a typical Gaussian frequency distribution with a center  $f_m$ , a half width  $\delta f$ , a band between  $f_1$  and  $f_2$ <sup>30</sup>.

$$B_f^2 = \frac{2B_1^2}{\sqrt{\pi}\delta f} \left[ \operatorname{erf} \left( \frac{f_2 - f_m}{\delta f} \right) + \operatorname{erf} \left( \frac{f_m - f_1}{\delta f} \right) \right]^{-1} \exp \left[ -\frac{(f - f_m)^2}{(\delta f)^2} \right] \quad (4)$$

here  $B_1$  is the wave amplitude in units of Tesla and erf is the error function.

We choose the wave normal angle distribution to also satisfy a standard Gaussian form:

$$g(X) \propto \begin{cases} \exp[-(X - X_m)/X_o]^2 & \text{for } X_1 \leq X \leq X_2, \\ 0 & \text{otherwise,} \end{cases} \quad (5)$$

where  $X = \tan \theta$  ( $\theta_1 \leq \theta \leq \theta_2$ ,  $X_{1,2} = \tan \theta_{1,2}$ ), with a half-width  $X_o$ , and a peak  $X_m$ . Based on the observation, we choose  $X_m = \tan 89^\circ$ ,  $X_o = \tan 86^\circ$ ,  $X_1 = X_m - X_o$ ,  $X_2 = X_m + X_o$ , and the maximum latitude for the presence of MS waves  $\lambda_m = 5^\circ$ . We assume that the wave spectral intensity remain constant along the dipolar geomagnetic field line.

As shown in Figure 3, there is a cross region between two bands with the cross frequency  $f_{cr} = 70$  Hz. We consider contribution from harmonic resonances up to  $n = \pm 20$  for the lower band and  $n = \pm 30$  for the upper band. To avoid repeating calculation from the cross region of two bands, the lower band stops at  $f_{cr} = 70$  Hz; and the upper band starts at  $f_{cr} = 70$  Hz. We then compute MS-driven bounce-averaged diffusion coefficients at the location  $L = 4.6$ .

The evolution of the proton phase space density  $f$  is calculated by solving the bounce-averaged pitch angle and momentum diffusion equation

$$\frac{\partial f}{\partial t} = \frac{1}{Gp} \frac{\partial}{\partial \alpha_e} \left[ G \left( \langle D_{zz} \rangle \frac{1}{p} \frac{\partial f}{\partial \alpha_e} + \langle D_{zp} \rangle \frac{\partial f}{\partial p} \right) \right] + \frac{1}{G} \frac{\partial}{\partial p} \left[ G \left( \langle D_{pz} \rangle \frac{1}{p} \frac{\partial f}{\partial \alpha_e} + \langle D_{pp} \rangle \frac{\partial f}{\partial p} \right) \right] \quad (6)$$

here  $p$  is the proton momentum,  $G = p^2 T(\alpha_e) \sin \alpha_e \cos \alpha_e$  with  $\alpha_e$  being the equatorial pitch angle, the normalized bounce time  $T(\alpha_e) \approx 1.30 - 0.56 \sin \alpha_e$ ;  $\langle D_{zz} \rangle$ ,  $\langle D_{pp} \rangle$ , and  $\langle D_{zp} \rangle = \langle D_{pz} \rangle$  denote bounce-averaged diffusion coefficients in pitch angle, momentum and cross pitch angle-momentum. The explicit expressions of those bounce-averaged diffusion coefficients for MS waves can be found in the previous work<sup>24,25</sup>.

The initial condition is modeled by a kappa-type distribution function of energetic protons<sup>31</sup>:

$$f_0^\kappa(p, \sin \alpha_e) = \frac{n_p \Gamma(\kappa + l + 1)}{\pi^{3/2} \theta_e^3 \kappa^{l+3/2} \Gamma(l+1) \Gamma(\kappa - 1/2)} \left( \frac{p \sin \alpha_e}{\theta} \right)^{2l} \left[ 1 + \frac{p^2}{\kappa \theta^2} \right]^{-(\kappa + l + 1)} \quad (7)$$

here  $n_p$ ,  $l$ ,  $\kappa$ , and  $\Gamma$  denote the number density of energetic protons, the loss-cone index, the spectral index, and the gamma function.  $\theta_e^2$  represents the effective thermal parameter normalized by the proton rest mass energy  $m_p c^2$  ( $\sim 938$  MeV).

Solution of the diffusion equation (6) requires to choose the appropriate and realistic initial and boundary conditions in order for a realistic simulation of this event. Boundary conditions in pitch angle are taken:  $f = 0$  at the loss-cone  $\alpha_e = \alpha_L$  (sin  $\alpha_L = L^{-3/2}(4 - 3/L)^{-1/4}$ ) to simulate a rapid precipitation of protons inside the loss cone (Fig. 1d), and  $\partial f / \partial \alpha_e = 0$  at  $\alpha_e = 90^\circ$ . For the energy boundary conditions,  $f$  is assumed to remain constant at the lower boundary 0.5 keV and the upper boundary 20 keV, respectively.

Based on the observational data, we choose the following values of parameters:  $\theta_e^2 = 0.5 \times 10^{-6}$  ( $\sim 5$  keV),  $l = 0.01$ ,  $\kappa = 3$  and  $n_p = 2.9 \text{ cm}^{-3}$ . We solve the equation using the recently developed hybrid difference method<sup>25</sup>, which is efficient, stable and

easily parallel programmed. The numerical grid is set to be  $91 \times 101$  and uniform in pitch angle and natural logarithm of momentum.

- Gérard, J.-C. *et al.* Observation of the proton aurora with IMAGE FUV imager and simultaneous ion flux in situ measurements. *J. Geophys. Res.* **106**, 28939–28948 (2001).
- Frey, H. U. *et al.* The electron and proton aurora as seen by IMAGE-FUV and FAST. *Geophys. Res. Lett.* **28**, 1135–1138 (2001).
- Summers, D., Thorne, R. M. & Xiao, F. Relativistic theory of wave-particle resonant diffusion with application to electron acceleration in the magnetosphere. *J. Geophys. Res.* **103**, 20487–20500 (1998).
- Erlanson, R. E. & Ukhorskiy, A. J. Observations of electromagnetic ion cyclotron waves during geomagnetic storms: Wave occurrence and pitch angle scattering. *J. Geophys. Res.* **106**, 3883 (2001).
- Sakaguchi, K. *et al.* Simultaneous appearance of isolated auroral arcs and Pc 1 geomagnetic pulsations at subauroral latitudes. *J. Geophys. Res.* **113**, A05201 (2008).
- Xiao, F. *et al.* Determining the mechanism of cusp proton aurora. *Sci. Rep.*, **3**, 1654 (2013).
- Horne, R. B. & Thorne, R. M. On the preferred source location for the convective amplification of ion cyclotron waves. *J. Geophys. Res.* **98**, 9233 (1993).
- Jordanova, V. K. *et al.* Modeling ring current proton precipitation by electromagnetic ion cyclotron waves during the May 14–16, 1997, storm. *J. Geophys. Res.* **106**, 7 (2001).
- Chen, L., Thorne, R. M. & Horne, R. B. Simulation of EMIC wave excitation in a model magnetosphere including structured high-density plumes. *J. Geophys. Res.* **114**, A07221 (2009).
- Anderson, B. J., Erlanson, R. E. & Zanetti, L. J. A statistical study of Pc 1–2 magnetic pulsations in the equatorial magnetosphere. 1. Equatorial occurrence distributions. *J. Geophys. Res.* **97**, 3075–3088 (1992).
- Usanova, M. E., Mann, I. R., Bortnik, J., Shao, L. & Angelopoulos, V. THEMIS observations of electromagnetic ion cyclotron wave occurrence: Dependence on AE, SYMH, and solar wind dynamic pressure. *J. Geophys. Res.* **117**, A10218 (2012).
- Keika, K., Takahashi, k., Ukhorskiy, A. Y. & Miyoshi, Y. Global characteristics of electromagnetic ion cyclotron waves: Occurrence rate and its storm dependence. *J. Geophys. Res.: Space Physics*, **118**, 4135–4150 (2013).
- Santolík, O., Pickett, J. S., Gurnett, D. A., Maksimovic, M. & Cornilleau-Wehrin, N. Spatiotemporal variability and propagation of equatorial noise observed by cluster. *J. Geophys. Res.* **107**, 1495 (2002).
- Meredith, N. P., Horne, R. B. & Anderson, R. R. Survey of magnetosonic waves and proton ring distributions in the earth's inner magnetosphere. *J. Geophys. Res.* **113**, A06213 (2008).
- Chen, L., Thorne, R. M., Jordanova, V. K., Thomsen, M. F. & Horne, R. B. Magnetosonic wave instability analysis for proton ring distributions observed by the LANL magnetospheric plasma analyzer. *J. Geophys. Res.* **116**, A03223 (2011).
- Xiao, F., Zhou, Q., He, Z. & Tang, L. Three-dimensional ray tracing of fast magnetosonic waves. *J. Geophys. Res.* **117**, A06208 (2012).
- Horne, R. B. *et al.* Electron acceleration in the Van Allen radiation belts by fast magnetosonic waves. *Geophys. Res. Lett.* **34**, L17107 (2007).
- Mende, S. B. *et al.* Far ultraviolet imaging from the IMAGE spacecraft, 3, Spectral imaging of Lyman-alpha and OI 135.6 nm. *Space Sci. Rev.* **91**, 271 (2000).
- Frey, H. U. *et al.* Proton aurora in the cusp. *J. Geophys. Res.* **107**, 1091 (2002).
- Fuselier, S. A. *et al.* Cusp aurora dependence on interplanetary magnetic field Bz. *J. Geophys. Res.* **107**, 1111 (2002).
- Horne, R. B. Path-integrated growth of electrostatic waves: The generation of terrestrial myriametric radiation. *J. Geophys. Res.* **94**, 8895–8909 (1989).
- Xiao, F., Chen, L., Zheng, H. & Wang, S. A parametric ray tracing study of superluminous auroral kilometeric radiation wave modes. *J. Geophys. Res.* **112**, A10214 (2007).
- Thorne, R. M., Ni, B., Tao, X., Horne, R. B. & Meredith, N. P. Scattering by chorus waves as the dominant cause of diffuse auroral precipitation. *Nature* **467**, 943–946 (2010).
- Glauert, S. A. & Horne, R. B. Calculation of pitch angle and energy diffusion coefficients with the PADIE code. *J. Geophys. Res.* **110**, A04206 (2005).
- Xiao, F., Su, Z., Zheng, H. & Wang S. Modeling of outer radiation belt electrons by multidimensional diffusion process. *J. Geophys. Res.* **114**, A03201 (2009).
- Ma, Q., Li, W., Thorne, R. M. & Angelopoulos, V. Global distribution of equatorial magnetosonic waves observed by THEMIS. *Geophys. Res. Lett.*, **40**, 1895–1901 (2013).



27. Xiao, F. *et al.* Magnetosonic wave instability by proton ring distributions: Simultaneous data and modeling. *J. Geophys. Res.* **118**, 4053 (2013).
28. Suchy, K. Real Hamilton equations of geomagnetic optics for media with moderate absorption. *Radio Sci.*, **16**, 1179 (1981).
29. Gallagher, D. L., Craven, P. D. & Comfort, R. H. Global core plasma model. *J. Geophys. Res.* **105**, 18819–18833 (2000).
30. Lyons, L. R., Thorne, R. M. & Kennel, C. F. Pitch angle diffusion of radiation belt electrons within the plasmasphere. *J. Geophys. Res.*, **77**, 3455–3474 (1972).
31. Vasyliunas, V. M. A survey of low-energy electrons in the evening sector of the magnetosphere with ogo 1 and ogo 3. *J. Geophys. Res.*, **73**, 2839–2884 (1968).

## Acknowledgments

This work is supported by 973 Program 2012CB825603, the National Natural Science Foundation of China grants 41274165, 41204114, the Aid Program for Science and Technology Innovative Research Team in Higher Educational Institutions of Hunan Province, and the Construct Program of the Key Discipline in Hunan Province.

## Author contributions

F.L.X. and Q.G.Z. led the idea and modelling, Y.F.W. and Z.G.H. contributed data analysis and interpretation, Z.P.S., C.Y. and Q.H.Z. contributed modelling.

## Additional information

**Competing financial interests:** The authors declare no competing financial interests.

**How to cite this article:** Xiao, F.L. *et al.* Generation of proton aurora by magnetosonic waves. *Sci. Rep.* **4**, 5190; DOI:10.1038/srep05190 (2014).



This work is licensed under a Creative Commons Attribution-NonCommercial-NoDerivs 4.0 International License. The images or other third party material in this article are included in the article's Creative Commons license, unless indicated otherwise in the credit line; if the material is not included under the Creative Commons license, users will need to obtain permission from the license holder in order to reproduce the material. To view a copy of this license, visit <http://creativecommons.org/licenses/by-nc-nd/4.0/>